Available online at www.sciencedirect.com

SciVerse ScienceDirect

Ceramics International 38 (2012) 3301–3307

CERAMICS INTERNATIONAL

www.elsevier.com/locate/ceramint

C/C–SiC composite prepared by Si–10Zr alloyed melt infiltration

Yonggang Tong *, Shuxin Bai, Hong Zhang, Ke Chen

College of Aerospace and Materials Engineering, National University of Defense Technology, Changsha 410073, PR China

Received 19 August 2011; received in revised form 16 December 2011; accepted 16 December 2011
Available online 27 December 2011

Abstract

A high performance and low cost C/C–SiC composite was prepared by Si–10Zr alloyed melt infiltration. Carbon fiber felt was firstly densified by pyrolytic carbon using chemical vapor infiltration to obtain a porous C/C preform. The eutectic Si–Zr alloyed melt (Zr: 10 at.%, Si: 90 at.%) was then infiltrated into the porous preform at 1450 °C to prepare the C/C–SiC composite. Due to the in situ reaction between the pyrolytic carbon and the Si–Zr alloy, SiC, $ZrSi_2$ and ZrC phases were formed, the formation and distribution of which were investigated by thermodynamics. The as-received C/C–SiC composite, with the flexural strength of 353.6 MPa, displayed a pseudo-ductile fracture behavior. Compared with the C/C preform and C/C composite of high density, the C/C–SiC composite presented improved oxidation resistance, which lost 36.5% of its weight whereas the C/C preform lost all its weight and the high density C/C composite lost 84% of its weight after 20 min oxidation in air at 1400 °C. ZrO_2, $ZrSiO_4$ and SiO_2 were formed on the surface of the C/C–SiC composite, which effectively protected the composite from oxidation.

Keywords: B. Composites; C. Mechanical properties; D. SiC; Microstructure

1. Introduction

Ceramic matrix composites, reinforced by high strength continuous ceramic fibers, have attracted much attention for high temperature structural applications because of their superior high temperature strength, low density and improved damage tolerance [1,2]. Particularly, carbon fiber reinforced C, SiC binary matrix composite (C/C–SiC) is a promising material owing to its low density, high hardness, excellent oxidation resistance, high strength and thermal shock resistance [3,4]. It is a potential candidate for highly demanding engineering applications such as heat shields, structural components for reentry space vehicles, high performance brake discs and high temperature heat exchanger tubes [5].

Various techniques such as chemical vapor infiltration (CVI) [6], polymer impregnation and pyrolysis (PIP) [7,8], and reactive melt infiltration (RMI) [9] have been utilized to fabricate C/C–SiC composite. However, some of these processes have obvious disadvantages such as time-consuming, high-cost and reduction in strength for the obtained component at elevated temperatures [9]. PIP is a practical process to prepare C/C–SiC composite, yet the cost is quite high. The precursor is expensive and lots of cycles are usually needed to densify a sample. CVI is a common process, but it is time consuming, often taking hundreds of hours to densify a large sample. Reactive melt infiltration (RMI), by contrast, is an effective fabrication route with many advantages including short fabrication period, low cost, near net shape, etc. However, a certain amount of residual silicon often exists in the C/C–SiC composite prepared by RMI, which leads to potential degradation of the flexural strength [10]. In addition, the working temperature of the composite is limited by the softening of the residual silicon. To overcome the problem of residual silicon, the porous C/C preform could be infiltrated with an alloyed melt of silicon [11,12]. Si–Mo [13,14], Si–Nb [15] and Si–Mo–Ti [16] alloyed melts have been used to fabricate C/C–SiC composites by RMI. The residual silicon was eliminated and the composites demonstrated improved performances.

However, the maximum working temperature of silicon based ceramics is limited to about 1600 °C due to the onset of active oxidation in dry air and to even lower temperatures in water vapor environments [17]. Introduction of ultra-high temperature ceramics (UHTCs) such as refractory carbides,

* Corresponding author. Tel.: +86 731 4576147; fax: +86 731 4574791.
E-mail address: tygiaarh419@163.com (Y. Tong).

0272-8842/$36.00
doi:10.1016/j.ceramint.2011.12.038

borides and silicides into C/C–SiC composites allows the composites to be used as potential candidates for extreme environments associated with the hypersonic flight and rocket propulsion due to their retained strength and ablation resistance at temperatures over 1600 °C [18]. Among the family of UHTCs, zirconium-bearing UHTCs, due to their high melting temperatures and relatively low density, are of great interest, the oxides of which formed in the ablation and oxidation processes can effectively reduce the diffusion rate of oxidizing atmosphere. Great efforts have been made to introduce zirconium-bearing UHTCs into C/C–SiC composite [17,19,20]. The aim of the present work is to prepare a low cost C/C–SiC composite by Si–10Zr alloyed melt infiltration. For one hand, zirconium is added into the silicon melt to eliminate the residual silicon, for the other, zirconium in the melt is expected to react with carbon and silicon to form zirconium carbides and silicides, which will improve the composite performance.

2. Experimental

Carbon fiber needled felts were used as preforms. The carbon fibers were PAN-based (T300, Toray, Japan). The needled felts were prepared by a three-dimensional needling technique, starting with repeatedly overlapping the layers of 0° non-woven fiber cloth, short-cut-fiber web, and 90° non-woven fiber cloth with needle-punching step by step. Pyrolytic carbon was deposited on the surface of the carbon fibers as the reaction carbon by chemical vapor infiltration. The porous C/C preform were cut, polished, ultrasonically cleaned with ethanol and dried at 100 °C for 4 h in an oven. A piece of Si–Zr alloy (Si: 90 at.%, Zr: 10 at.%) was then placed on top of the C/C preform in a graphite pot, and the pot was put into a high temperature furnace. The sample was heated to 1450 °C and kept for 1 h followed by furnace cooling to prepare the C/C–SiC composite. The pressure in the furnace was kept constant below 5.0×10^{-2} Pa.

The apparent density of the composite was measured by Archimedes's method. Flexural strength was determined using a three-point-bending test on specimens of 50 mm × 10 mm × 4 mm with 40 mm span and 0.5 mm/min crosshead speed. The composite was heated in the calm air in a corundum tube furnace to investigate the isothermal oxidation behavior. The sample was put into the furnace at 1400 °C for 5 min, then taken out quickly.

Table 1
Density and porosity of the C/C preform and C/C–SiC composite.

	C/C preform	C/C–SiC composite
Density, g/cm^3	1.32	2.07
Open porosity, %	25.83	5.02

Weight changes of the sample were measured at room temperature by an electronic balance with a sensitivity of ±0.1 mg. Subsequently, the sample was put in the furnace again for the next thermal cycle.

The microstructures of the composite were observed by scanning electron microscopy using a JSM-6360LV instrument, at accelerating voltages in the range 5–25 kV. The chemical composition was determined by energy dispersive spectroscopy (EDS). The phase identification was conducted by X-ray diffraction (XRD, Rigaku D/Max 2550VB-) using a Ni-filtered Cu Kα radiation at a scanning rate of 5°/min and scanning from 10° to 80° of 2θ.

3. Results and discussion

3.1. Density and open porosity of C/C preforms and C/C–SiC composite

Table 1 lists the bulk density and open porosity of the C/C preform and the C/C–SiC composite. The density of the composite increased from 1.32 g/cm^3 to 2.07 g/cm^3, while the open porosity decreased from 25.83% to 5.02% after RMI. It is indicated that the Si–Zr melt infiltrated into the C/C preform very well after RMI, the pores in the preform were filled and a dense matrix was formed, which could be also confirmed by observing the microstructure of the C/C–SiC composite (Fig. 1). The density of silicon–zirconium alloy is about 3.1 g/cm^3 while the C/C preform density is 1.32 g/cm^3, so the density of the composite increased after RMI.

3.2. Microstructure and composition of the composite

Fig. 1 shows the backscattered electron micrographs of the obtained C/C–SiC composite. It is observed that the alloyed Si–Zr melt has infiltrated into the large pores among adjacent carbon fiber bundles and some small pores among carbon fibers.

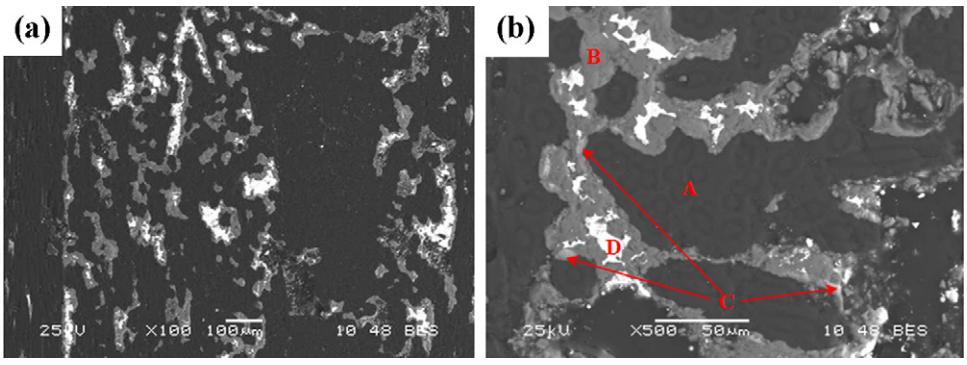

Fig. 1. Typical SEM micrographs of the C/C–SiC composite: (a) 30× and (b) 500×.

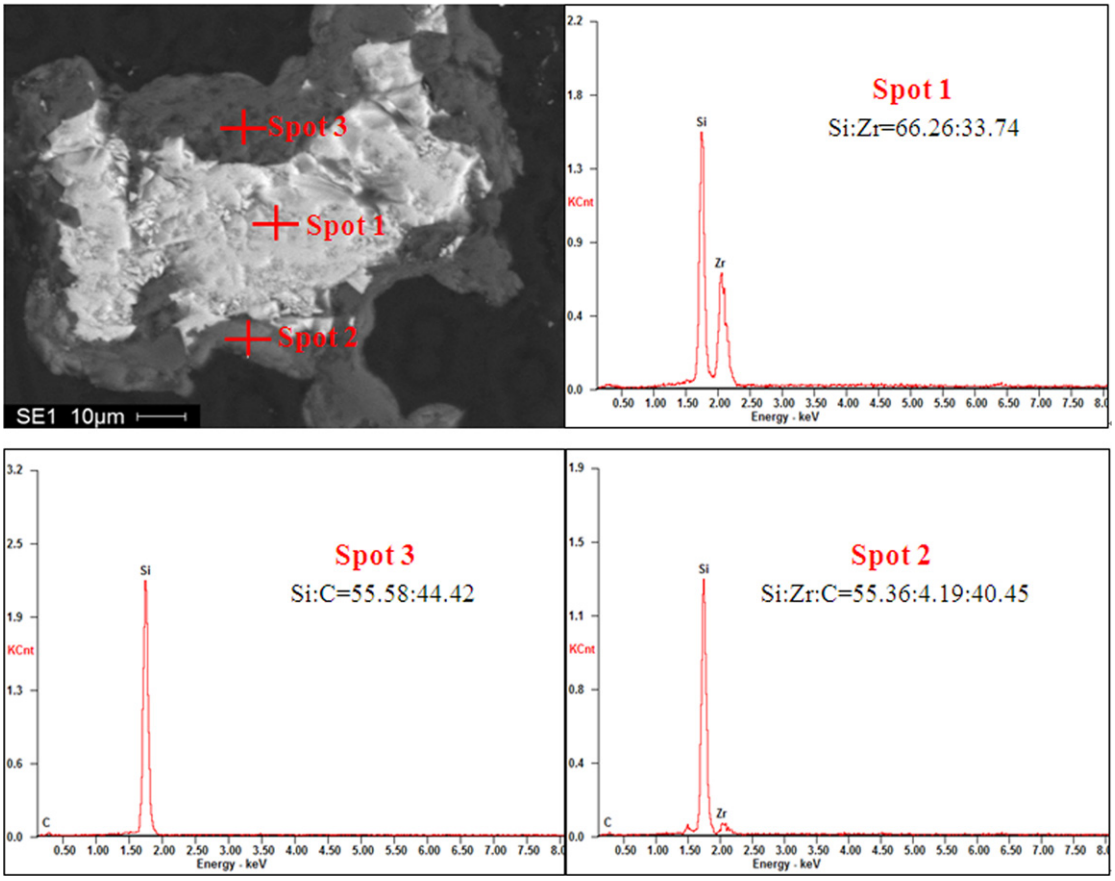

Fig. 2. EDS analysis of the C/C–SiC composite.

The composite is found to consist of four regions, namely the black, grey, hoar and white regions, which are marked as A, B, C and D in Fig. 1(b), respectively. EDS analysis (Fig. 2) reveals that the region B is composed of silicon and carbon, which is believed to be the phase SiC derived from the reaction between pyrolytic carbon and silicon. The hoar region C is composed of silicon, zirconium and carbon, which suggests the phases ZrC and SiC. The white region D may be $ZrSi_2$ which owns a constitution of Si:Zr = 66.26:33.74. The black region A composed of only carbon includes the presence of carbon fibers and the residual pyrolytic carbon. No region composed of residual silicon was found by EDS.

The results from EDS analysis are confirmed by the XRD analysis (Fig. 3), which indicates that the phases in the obtained

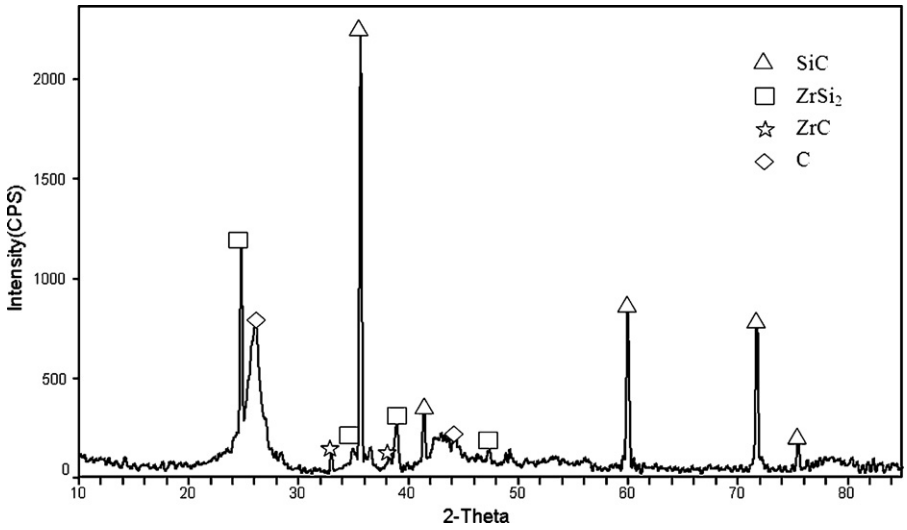

Fig. 3. XRD patterns of the C/C–SiC composite.

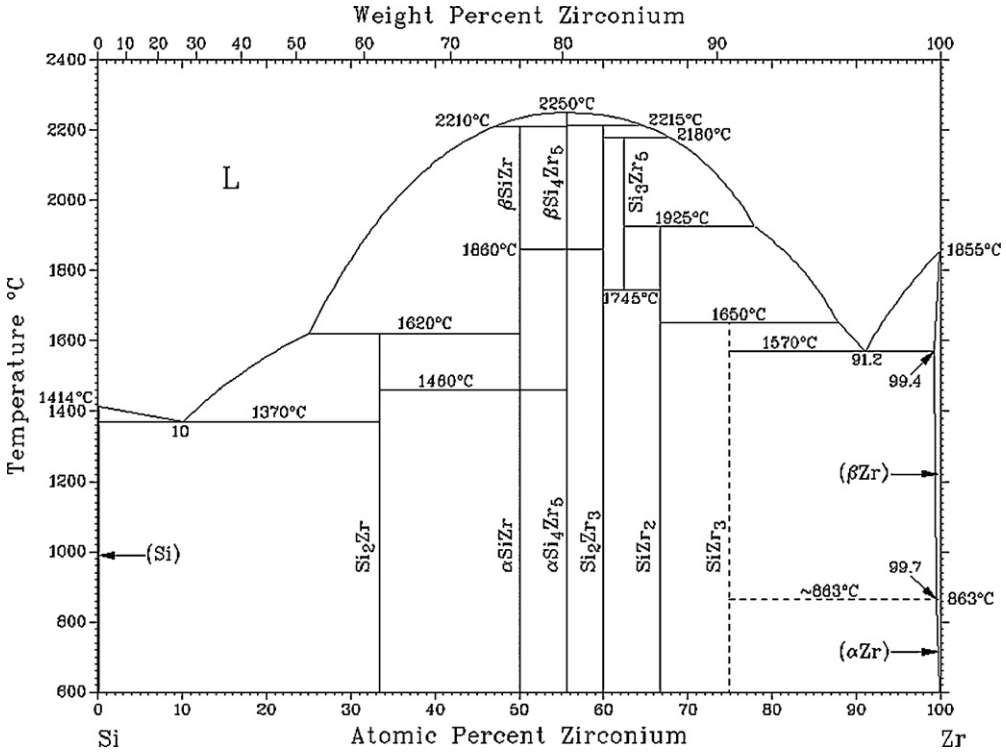

Fig. 4. Phase diagram of Si–Zr system.

composite are SiC, $ZrSi_2$, ZrC and carbon. No detectable silicon peaks was seen in the XRD patterns. The broad carbon-peaks refer to the carbon fibers and the residual pyrolytic carbon. The main phase SiC resulted from the reaction between silicon and pyrolytic carbon is of face centered cubic (fcc) type, i.e., β-SiC. In addition, a small amount of ZrC is formed due to the reaction between carbon and zirconium.

Fig. 1(b) reveals that SiC and ZrC were formed around the pyrolytic carbon after alloyed melt infiltration. The distribution of SiC was continuous whereas a small amount of discontinuous ZrC was just formed on the edge of pyrolytic carbon. It is believed that the formation and distribution of the phases in the composite may be concerned with the reaction ability of silicon and zirconium with carbon, respectively. The reactions and thermodynamic calculations are as follows:

$$C + Zr \rightarrow ZrC \quad \Delta G_{1450\,^{\circ}C} = -183.66\,kJ/mol \tag{1}$$

$$C + Si \rightarrow SiC \quad \Delta G_{1450\,^{\circ}C} = -62.52\,kJ/mol \tag{2}$$

Known from the thermodynamic calculations, the formation of ZrC according to Eq. (1) is more favorable than that of SiC according to Eq. (2) due to the much more negative Gibbs free energy. During the process of alloyed melt infiltration, Si–Zr melt homogenously infiltrates into the porous C/C preform. Zirconium in the melt prefers to react with pyrolytic carbon when the melt meets the pyrolytic carbon at the beginning. However, the zirconium (10 at.%) in the Si–Zr melt is not enough for the subsequent formation of ZrC, which leads to the small amount of discontinuous reaction-formed ZrC distributing around the pyrolytic carbon. Here, the reaction between silicon and carbon occurs and the phase SiC is formed. There is enough silicon in the Si–Zr melt, and more and more SiC is formed. The concentration of silicon in the melt decreases due to the reaction between silicon and carbon, and $ZrSi_2$ phase begins to solidify from the Si–Zr melt at a certain time, which is indicated by the phase diagram of Si–Zr system (Fig. 4). With the proceeding of the reaction between silicon and carbon, SiC and $ZrSi_2$ phases keep forming until both silicon and zirconium in the melt are completely consumed. Finally, the continuous SiC and discontinuous ZrC and $ZrSi_2$ are developed in the composite, in which the continuous SiC and discontinuous ZrC distribute around the pyrolytic carbon inside the pores of the C/

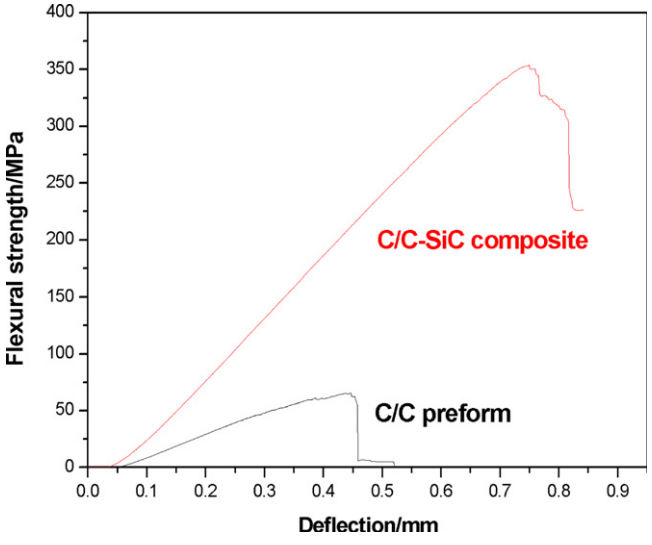

Fig. 5. Typical stress–deflection curves for the C/C preform and C/C–SiC composite.

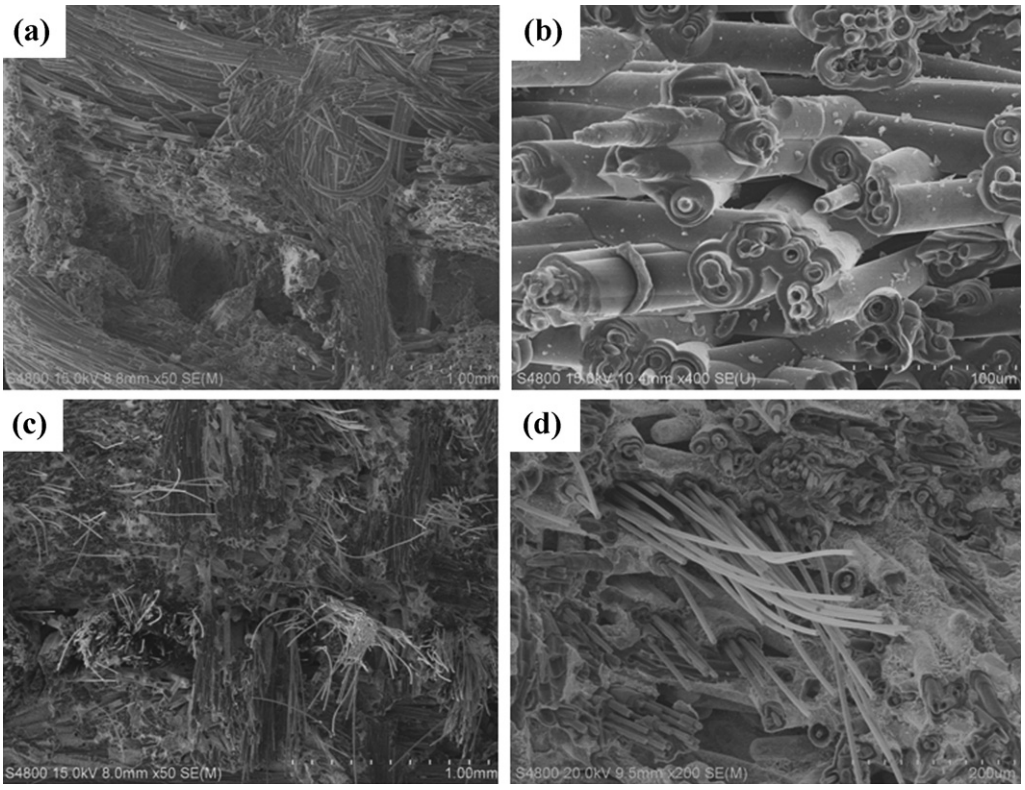

Fig. 6. SEM photographs of the fracture surfaces: (a) and (b) C/C preform, (c) and (d) C/C–SiC composite.

C preform and the $ZrSi_2$ locates in the middle of pores surrounded by the SiC.

3.3. Mechanical properties

Typical stress–deflection curves derived from the bending test for the C/C preform and the C/C–SiC composite are shown in Fig. 5. The flexural strength of the C/C–SiC composite is 353.6 MPa, which is much higher than that of the C/C preform, 65.5 MPa. For the C/C–SiC composite, the curve shows that an initial quasi-linear elastic region is followed by an increasing nonlinear stress up to a maximum. After reaching the maximum value, the stress decreases gradually. It shows a pseudo-ductile fracture behavior. Compared with the C/C–SiC composite, the C/C preform just shows a quasi-linear elastic region, followed by a sharp decrease of the stress after it reaches a maximum value.

The SEM photographs of the fracture surfaces for the C/C preform and the C/C–SiC composite are shown in Fig. 6. It shows that there are lots of pores in the C/C preform. The big pores exist among the carbon fiber bundles and the small pores exist inside the carbon fiber bundles (Fig. 6(a) and (b)). After alloyed melt infiltration, both types of pores are filled and the preform is greatly densified (Fig. 6(c)), which plays a key role in stress transferring. Upon loading, stress can be effectively transferred from the dense matrix to the residual pyrolytic carbon and the carbon fibers. As a result, the dense C/C–SiC composite shows improved mechanical properties.

Fig. 6(b) presents that the pyrolytic carbon possesses good adherence to the carbon fibers in the C/C preform, which tends to result in a brittle fracture behavior. Cracks formed within the matrix cannot be stopped or deflected around the carbon fibers, thus the C/C preform presents a flat fracture surface with a sharp load decrease in the stress–deflection curves. Compared with the C/C preform, the C/C–SiC composite has much lower content of residual pyrolytic carbon and some ZrC and SiC phases are formed around the pyrolytic carbon. The residual pyrolytic carbon presents lower adherence to carbon fibers after alloyed melt infiltration, and the reaction-formed ZrC and SiC do not adhere to the residual pyrolytic carbon tightly because of the large mismatch of the coefficient of thermal expansion between pyrolytic carbon, SiC and ZrC (CTE_C = 1.2 ppm/K, CTE_{SiC} = 4.3 ppm/K, CTE_{ZrC} = 6.9 ppm/K). For the C/C–SiC composite, therefore, the carbon fibers tend to split from the matrix and cracks formed in the matrix deflect along the interfaces with lower adherence. Thus, the C/C–SiC composite is toughed and shows a pseudo-ductile fracture behavior.

3.4. Oxidation resistance properties

The results of the isothermal oxidation tests in the air at 1400 °C are shown in Fig. 7. The weight loss–time curves evidently reveal that the obtained C/C–SiC composite shows much better oxidation resistance compared with the C/C preform (density: 1.32 g/cm^3) and the C/C composite (density: 1.8 g/cm^3). After 20 min oxidation, the C/C–SiC composite lost 36.5% of its weight whereas the C/C preform lost all its weight and the high density C/C composite lost 84% of its weight. XRD phase analysis of the C/C–SiC composite after oxidation is shown in Fig. 8. It is indicated that ZrO_2, SiO_2 and $ZrSiO_4$ phases are formed on the surface of the composite.

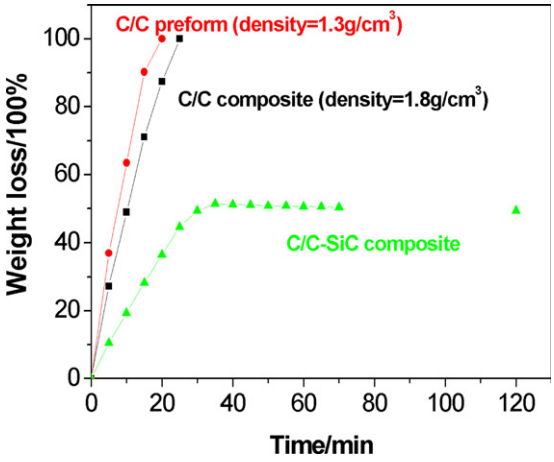

Fig. 7. Oxidation curve of weight loss on time at 1400 °C of C/C–SiC and C/C composites.

The oxidation curve of the C/C–SiC composite in Fig. 7 can be divided into four segments: linear rise, non-linear rise, slow non-linear decrease and flat displacement, corresponding to four stages of oxidation. The oxidation of carbon loses weight, yet the oxidation of ZrC, $ZrSi_2$ and SiC gets weight. At the beginning, the oxidation of the composite is of reaction control due to the fast diffusion of oxygen. There is the most amount of carbon (including carbon fibers and pyrolytic carbon) exposed in the air, the oxidation rate of which is quite large at 1400 °C. Compared with the weight loss from carbon oxidation, the weight gain resulting from the oxidation of SiC, ZrC and $ZrSi_2$ can be ignored. The weight loss of the composite is controlled by the reaction of carbon with oxygen, which linearly increases with the oxidation time. After 20 min oxidation, the amount of bare carbon exposed in the air decreases and the weight gain from the oxidation of SiC, ZrC and $ZrSi_2$ cannot be ignored, which, however, is still smaller than the weight loss of carbon oxidation. The weight loss of the composite non-linearly increases with the oxidation time. After 35 min oxidation, much more amount of SiC, ZrC and $ZrSi_2$ is oxidized. SiO_2 resulting from the oxidation of SiC and $ZrSi_2$ is in liquid condition at 1400 °C, which can flow onto the surface of the bare carbon and protect the carbon form subsequent oxidation [21]. Here, the weight gain from the oxidation of SiC, ZrC and $ZrSi_2$ becomes larger than the weight loss from the carbon oxidation and the composite gets a slow non-linear weight gain. At a certain moment, the bare carbon in the composite is oxidized and sufficient SiO_2, $ZrSiO_4$ and ZrO_2 phases are formed on the composite, which serves as a layer to protect the composite from oxidation. At this stage, the composite oxidation begins to be controlled by oxygen diffusion through the protection layer [22,23]. Because the diffusion rate of oxygen in SiO_2, $ZrSiO_4$ and ZrO_2 is quite low, the oxidation rate of the composite is very low [24]. Therefore, no obvious weight loss was found and the oxidation curve presents flat displacement, i.e., the forth stage in the oxidation curve.

4. Conclusions

C/C–SiC composite was successfully prepared by alloyed melt infiltration. SiC, $ZrSi_2$ and ZrC phases were formed after the melt infiltration. No residual silicon was found by EDS and XRD analysis. The density of the obtained composite is 2.07 g/cm^3, and its open porosity is 5.02%. The flexural strength of the C/C–SiC composite is 353.6 MPa, which shows a pseudo-ductile fracture behavior with large numbers of fibers pulled out of the composite on the fracture surface. The oxidation resistance of the C/C–SiC composite is significantly improved compared with that of the C/C composite. After oxidation in air for 20 min at 1400 °C, the weight loss of the C/C–SiC composite is 36.5% whereas the C/C preform lost all its weight. Much better oxidation resistance for the C/C–SiC composite is mainly due to the formation of ZrO_2, $ZrSiO_4$ and SiO_2 on the surface of the composite, which effectively prohibited the subsequent oxidation of the composite.

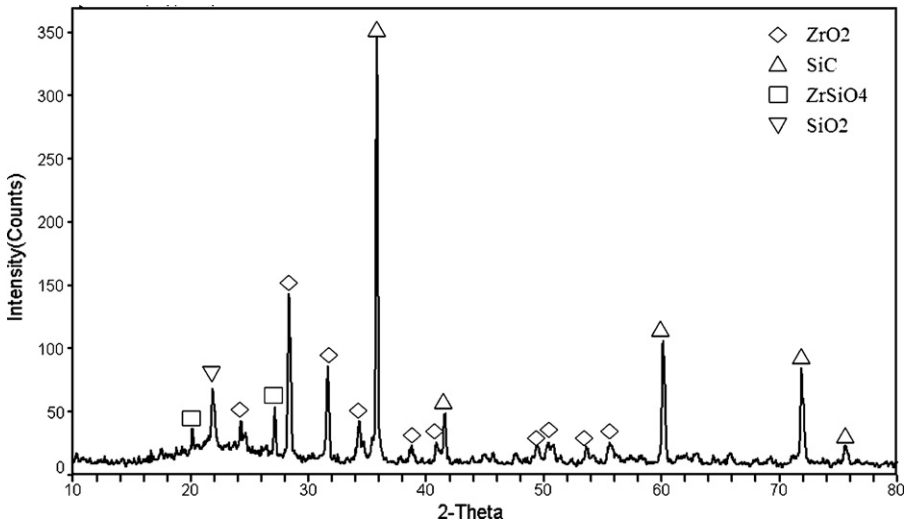

Fig. 8. XRD patterns of C/C–SiC composite after oxidation.

References

[1] M.H. Van de Voorde, M.R. Nedele, CMC's research in Europe and the future of CMC's in industry, Ceram. Eng. Sci. Proc. 17 (4) (1996) 3–7.

[2] R. Naslain, Design, preparation and properties of non-oxide CMCs for application in engines and nuclear reactors: an overview, Compos. Sci. Technol. 64 (2004) 155–170.

[3] W. Krenkel, Application of fiber reinforced C/C–SiC ceramic, Ceram. Forum. Int. 80 (8) (2003) 31–38.

[4] B. Manuel, Advanced ceramic materials for high temperature applications, Adv. Eng. Mater. 8 (8) (2006) 693–703.

[5] R.E. Tressler, Recent developments in fibers and interphases for high temperature ceramic matrix composites, Compos. A 30 (1999) 429–437.

[6] R. Naslain, R. Pailler, X. Bourrat, S. Bertarnd, L. Lamouroux, Synthesis of highly tailored ceramic matrix composites by pressure-pulsed CVI, Solid State Ionics 541 (2001) 141–144.

[7] K. Sato, A. Tezuka, O. Funayama, T. Isoda, Y. Terada, S. Kato, et al., Fabrication and pressure testing of a gas-turbine component manufactured by a pre ceramic–polymer-impregnation method, Compos. Sci. Technol. 59 (1999) 853–859.

[8] A. Kohyama, M. Kotani, Y. Katoh, T. Nakayasu, M. Sato, T. Yamamura, et al., High performance SiC/SiC composites by improved PIP processing with new precursor polymers, J. Nucl. Mater. 283 (2000) 565–569.

[9] S.Z. Jiang, X. Xiong, Z.K. Chen, P. Xiao, B.Y. Huang, Influence factors of C/C–SiC dual matrix composites prepared by reactive melt infiltration, Mater. Des. 30 (2009) 3738–3742.

[10] G.G. Trantina, R.L. Mehan, High-temperature time-dependent strength of an Si/SiC composite, J. Am. Ceram. Soc. 3 (60) (1977) 177–178.

[11] M. Singh, R.M. Dickerson, Characterization of SiC fiber (SCS-6) reinforced-reaction-formed silicon carbide matrix composites, J. Mater. Res. 11 (3) (1996) 746–751.

[12] J. Yang, O.J. Ilegbusi, Kinetics of silicon-metal alloy infiltration into porous carbon, Compos. A 31 (2000) 617–625.

[13] R.P. Messner, Y.M. Chiang, Liquid-phase reaction-bonding of silicon carbide using alloyed silicon-molybdenum melts, J. Am. Ceram. Soc. 73 (1990) 1193–1200.

[14] M. Singh, D.R. Behrendt, Reactive melt infiltration of silicon-molybdenum alloys into microporous carbon preforms, Mater. Sci. Eng. A 194 (1995) 193–200.

[15] M. Singh, D.R. Behrendt, Reactive melt infiltration of silicon–niobium alloys in microporous carbons, J. Mater. Res. 7 (1994) 1701–1709.

[16] M. Esfehanian, J.G. unster, F. Moztarzadeh, J.G. Heinrich, Development of a high temperature Cf/XSi_2–SiC (X = Mo, Ti) composite via reactive melt infiltration, J. Eur. Ceram. Soc. 27 (2007) 1229–1235.

[17] Z. Wang, S.M. Dong, Y.S. Ding, X.Y. Zhang, H.J. Zhou, J.S. Yang, et al., Mechanical properties and microstructures of C/SiC–ZrC composites using T700SC carbon fibers as reinforcements, Ceram. Int. 37 (2011) 695–700.

[18] S.F. Tang, J.Y. Deng, S.J. Wang, W.C. Liu, K. Yang, Ablation behaviors of ultra-high temperature ceramic composites, Mater. Sci. Eng. A 465 (2007) 1–7.

[19] N. Padmavathi, S. Kumari, V.V. Bhanu Prasad, J. Subrahmanyama, K.K. Ray, Processing of carbon–fiber reinforced (SiC + ZrC) mini-composites by soft-solution approach and their characterization, Ceram. Int. 35 (2009) 3447–3454.

[20] H.B. Li, L.T. Zhang, L.F. Cheng, Y.G. Wang, Fabrication of 2D C/ZrC–SiC composite and its structural evolution under high-temperature treatment up to 1800 °C, Ceram. Int. 35 (2009) 2831–2836.

[21] R. Naslain, A. Guette, F. Rebillat, S. Legallet, F. Lamouroux, L. Filipuzzi, et al., Oxidation mechanisms and kinetics of SiC-matrix composites and their constituents, J. Mater. Sci. 39 (2004) 7303–7316.

[22] F. Lamouroux, X. Bourrat, R. Naslain, Silicon carbide infiltration of porous C/C composites for improving oxidation resistance, Carbon 33 (4) (1995) 525–535.

[23] F. Lamouroux, X. Bourrat, R. Naslain, Kinetics and mechanisms of oxidation of 2D woven C/SiC composites: I, experimental approach, J. Am. Ceram. Soc. 77 (8) (1994) 2048–2057.

[24] J.F. Huang, X.R. Zeng, H.J. Li, X.B. Xiong, G.L. Sun, ZrO_2–SiO_2 gradient multilayer oxidation protective coating for SiC coated carbon/carbon composites, Surf. Coat. Technol. 190 (2005) 255–259.